Australian Earthquake Engineering Society
2024 National Conference, 21-23 November 2024
Adelaide, South Australia

Structure of Neotectonic Faulting and Earthquake Magnitude Potential of the Northeastern Eyre Peninsula

Ambica Sharma[1], Mark Quigley[1], James La Greca[1], Schirin Sellmann[1], Dan Clark[2]

1. School of Geography, Earth, and Atmospheric Science, The University of Melbourne, Parkville, VIC 3010

2. Geoscience Australia, 101 Jerrabomberra Ave, Symonston ACT 2609.

Abstract

The Eyre Peninsula region of South Australia hosts critical infrastructure and is an important mineral and gas resources region, including hydrogen and helium exploration. The northeastern part of Eyre Peninsula contains complex neotectonic faults that displace Quaternary units. Understanding these features is essential for reducing uncertainty in seismic hazard assessment. We use geospatial and geomorphic analysis of (i) high resolution drone-based photogrammetric digital elevation models (DEMs), (ii) lidar DEMs, and (iii) 30 m ALOS and 12 m TanDEM-X data to map the neotectonic fault traces and their relationships to displaced geological units and landforms, providing a refined understanding of Quaternary faulting in Eyre Peninsula. We employed multiple scaling relationships developed for faults in stable continental region to calculate maximum credible earthquake magnitudes (M_w max). By acknowledging the presence of epistemic uncertainties associated with various fault source parameters such as surface rupture lengths, fault dips, down-dip rupture width and area, we have strengthened the reliability and robustness of our results. Moreover, we find a strong correlation between the underlying crustal fabric and the geometry of Eyre Peninsula faults, implying the key role inherited structures play in fault propagation. Our analysis highlights the importance of high-resolution data in refining neotectonic fault mapping in the Eyre Peninsula. The data obtained from these comprehensive analyses will directly contribute to the development of a 3D fault source model of South Australia and ultimately contribute to Probabilistic Seismic Hazard Analyses (PSHA) and Probabilistic Fault Displacement Hazard Analyses (PFDHA) for the region.

Keywords: Neotectonics, Earthquakes, Eyre Peninsula, Intraplate faults

1. Introduction

Estimating moment magnitudes (M_W) from fault source parameters is a crucial step in developing robust seismic hazard analyses for a region, including Probabilistic Seismic Hazard Analyses (PSHA) and Probabilistic Fault Displacement Hazard Analyses (PFDHA). This assessment involves understanding the seismicity of active or neotectonic faults and characterizing them as seismic sources, which is important for evaluating ground shaking hazards (Chartier et al., 2017; Cornell, 1968). In contrast to plate boundary regions, where large earthquakes occur frequently, intraplate regions such as Australia, are often characterized by low seismicity and longer earthquake recurrence intervals (Crone & Machette, 1997; Crone et al., 2003; Clark et al., 2007). As a result, there is paucity in knowledge of the seismogenic characteristics of intraplate earthquakes with limited research on the underlying crustal structure, geology, and paleoseismology of known neotectonic faults. This leads to large uncertainties in estimating magnitude potentials for probabilistic seismic hazard analyses (Allen, 2020; Allen et al., 2023).

In intraplate regions, probabilistic hazard assessments present unique challenges including but not limited to the identification and characterization of rupture behaviour of neotectonic faults, short historical seismic records, and lack of comprehensive paleoseismic data. The current Australian national seismic hazard assessment (NSHA, 2023) incorporates various degrees of epistemic uncertainties in their fault source model by utilising weighted logic trees (Allen et al., 2023). However, the lack of directly measured source parameters from neotectonic faults across Australia leads to an incomplete understanding of magnitude potential and earthquake recurrence behaviour. Moreover, all historic surface ruptures with larger earthquakes have had no evidence of prior neotectonic rupture - and so could not have been identified by mapping prior to the event (e.g., King et al., 2019c; Clark et al., 2014; Crone et al., 1993; Machette et al., 1993). This leads to a pressing need to update the current fault source characterisation, as it directly informs building codes and design of critical infrastructure across Australia.

The Flinders Ranges Seismic Zone, regarded as one of the most seismically active zones in the Australian continent, has a remarkably well preserved neotectonic evidence of faulting (Sandiford, 2003; Crone et al., 2003; Quigley et al., 2006). While studies in the Flinders ranges (Célérier et al., 2005; Quigley et al., 2006) and more recently, the Nullarbor and Roe plains of South Australia and Western Australia (Sellmann et al., 2023) have informed the probabilistic seismic hazard analyses in South Australia (Allen et al., 2023), fewer studies have focused on quantifying paleoseismic parameters such as single-event displacements, magnitudes, and recurrence intervals in Eyre Peninsula, excluding the work of Crone et al. (2003), that have investigated neotectonic activity around the Roopena fault.

The Eyre Peninsula region hosts critical infrastructure and is gaining traction as an important mineral and gas resources region, including hydrogen and helium exploration (Alexander, 2023; Department of State Development, South Australia, n.d.). Previous studies on the Eyre Peninsula faults have demonstrated neotectonic activity and allow for the inference of activity rates to inform seismic hazard assessment models (Miles, 1952; Dunham, 1992; Crone et al., 2003; McCormack, 2006; Weatherman 2006). However, the existing studies are often incomplete investigations, lacking a comprehensive database for fault source parameters. Additionally, these studies may not adequately address the uncertainties associated with these parameters. Therefore, this study aims to improve the confidence of many inputs into the seismic hazard models for intraplate regions by producing an upgraded geospatial dataset of neotectonic faults in the eastern boundary of Eyre Peninsula, understanding the role of crustal architecture on the geometry of these ruptures, and producing weighted maximum credible moment magnitude estimates through scaling relationships derived for stable continental region faults.

2. Geology

The north-eastern Eyre Peninsula hosts a series of N-S and E-W trending fault scarps that sit in the Moonta subdomain of the eastern Gawler Craton (Parker et al., 1980). The en-echelon steps observed in these faults have been related to the concentration of stress at cratonic boundaries (Clark et al., 2012). Paleoproterozoic schists and granitic gneisses of the Lincoln Complex and Hutchinson Group form the basement hangingwall of the faults in the study area and have been deposited in a fluvial to shallow marine environment, before being involved in the Kimban orogeny to form the 200 km long Kalinjala Shear Zone (Parker and Lemon, 1982; Vassallo and Wilson, 2001; 2002). These basement rocks are uncomformably overlain by the shallow marine to non-marine Cenozoic Pirie Basin sediments (Parker and Fanning, 1998; Parker et al., 1985).

Drillhole records by BHP Minerals Ltd. (1983) classify one of the oldest sedimentary rocks in the region overlying the basement as the Kanaka Beds of Late Oligocene to Early Miocene age (Lindsay, 1970) with petroleum shales, and sand with pyritic lignite. Subsequently, widespread marine transgressions in the Miocene associated with the rifting of the Indo-Australian plate from Antarctica led to the deposition of the Melton Limestone (Lindsay, 1970; Ludbrook, 1959). Tertiary deposition in this region culminated with the deposition of non-fossiliferous lacustrine Gibbon beds in the Plio-Pleistocene (Miles, 1954; Alley and Lindsay, 1983); these beds are uncomformably overlain by the fluvial, erosional Quaternary deposits of the Randell formation (Jessup and Wright, 1971) capped by a calcrete layer (Dunham, 1992; Weatherman, 2006). Late Pleistocene alluvial sedimentation resulted in the widespread deposition of the Pooraka formation, a common Quaternary unit in the study area. Throughout the Holocene, aeolian quartz-rich sandy deposits known as Moornaba sands were uncomformably deposited over the southern and central part of the region (Parker, 1983a), visible in the topography as NW-SE trending longitudinal dunes that formed under semi-arid conditions in the landscape since the last glacial maximum (Thom et al., 1994).

3. Methods

3.1. Geospatial Mapping

We mapped the fault traces in the study area by utilizing a variety of datasets including digital elevation models (DEMs), 1:100,000 scale geological maps from South Australian Resources Information Gateway (SARIG), 1:250,000 scale geological map (Parker, 1983a), drillhole data (SARIG), and geophysical datasets including the total magnetic intensity map, also obtained from the Government of South Australia's SARIG online database. Broad scale mapping of the lineaments was done by using regional 1-arc second SRTM (30 m horizontal resolution) and TanDEM-X (12 m horizontal resolution) overlays along with high resolution drone-derived DEMs (10-20 cm pixel size) which aided in detailed, smaller scale mapping of selected study sites. Variably oriented scarp faces were accentuated in QGIS using different elevation-based hill shades and azimuth angles which led to more confident mapping of these structures. Subsequently, we categorized the lineaments on the basis of three confidence levels- definite, probable, and possible. Definite features were mapped as continuous and apparent traces, visible on the DEMs. Probable features were inferred traces that were not very prominent on the DEMs, typically due to topographic noise or obscured by erosional or depositional features. Possible features were those inferred traces that did not appear as distinct structures on the DEMs and/or bear no correlation with the trends of underlying geophysical lineaments, as observed for other historical Australian surface ruptures by Yang et al. (2021). Lastly, these mapped traces were also compared with the Australian Neotectonic Features Database (Clark and McPherson, 2012) and maps derived from unpublished research on the Eyre Peninsula faults (Dunham, 1992; Weatherman, 2006; McCormack, 2006).

3.2. Surface Rupture Lengths

We utilized our fault maps to calculate the surface rupture length of all the mapped faults using QGIS's inbuilt 'feature length' tool. We assumed surface rupture lengths comparable to subsurface rupture lengths for Eyre Peninsula faults following the findings by Yang et al. (2021) and King et al. (2019d) for Australian stable continental earthquakes. We calculated lengths for both 'tip to tip' ruptures and 'segmented' scenarios, identifying the individual segments based on their consistent strike, close proximity to other similar traces (≤ 2 km) (Matsuda, 1990), and absence of potential rupture barriers. We then defined the ends of a rupture trace by identifying if (i) the fault trace intersects another fault, and/or (ii) the fault trace changes strike by more than 25^0 (based on Biasi and Wesnousky, 2017), and/or (iii) if the fault geometry becomes complex and aligns with any pre-existing rupture barrier revealed by the total magnetic intensity dataset. Our 'Max length' values signify an ideal conceptual fault plane where we consider the length of all segments in a similar orientation and any obscured and/or inferred traces that may align with underlying geophysical lineaments along its strike. Note that this length may vary from the sum of identified segments and from our 'preferred length' scenarios. We assign our preferred rupture lengths assuming a complete tip-to-tip rupture with no rupture barriers. To account for fault bends, step-overs, splays, and strands, we calculate the preferred rupture length by simplifying fault geometry. A length uncertainty of 5 km is used to account for the poor discoverability in DEM data, and rupture complexity, based on the Australian fault source model (Clark et al., 2016).

3.3. Scaling Relationships

In order to estimate magnitude potentials for the Eyre Peninsula faults, we use four different scaling relationships involving surface rupture length (SRL) and fault rupture area (A). For length-scaled magnitude calculations, we have used the Yang et al. (2021) equation:

$$Log\ SRL = 0.5 * M_w - 1.93 \quad (1)$$

We have also used the Leonard (2014) equation:

$$M_w = a + b \times log\ SRL\ (where\ b = 1.667,\ a = 4.32) \quad (2)$$

These equations were used to estimate M_w potentials for preferred, maximum, and segmented rupture models.

For area-scaled magnitude calculations, we have used the Leonard (2014) equation:

$$M_w = a + b \times Log\ A\ (where\ b = 1.0,\ a = 4.19,\ A = rupture\ area\ in\ sq\ km) \quad (3)$$

We have also used the Somerville (2014) equation for stable continental region (SCR) earthquakes:

$$Log\ A = M_w - 4.25 \quad (4)$$

These scaling relationships utilise a comprehensive analysis of historical earthquake data, ranging from M_w 5.3 to 6.6, allowing for the derivation of robust empirical constants for dip-slip faults in stable continental regions.

Fault dip estimates were constrained by limited fault exposures and geometric analyses of fault traces using the rule of V's (Hanžl et al., 2019) in the topographic datasets. Where fault data was not available, we used an average estimated dip with 95% confidence of 45° ± 15, based on fault dips from known Australian surface rupturing earthquakes by King et al. (2019d). We have also inferred fault dips from the exposed mylonitic fabric of basement rocks along neotectonic fault traces in Eyre Peninsula that follow the same trend as the overlying fault scarps, assuming that the pre-existing zones of crustal weakness, as observed by Yang et al. (2021), and Sellmann et al. (2023), are prone to reactivation within the neotectonic stress field. Note that the dips for Eyre Peninsula faults are assumed to be the near-surface dips. These measurements justify the likely dip of the fault closer to the surface, and to account for the epistemic uncertainties in estimating mean fault dip from a limited number of measurements, we have applied a ±10° uncertainty range.

Down-dip rupture width estimates were calculated by using the 90th percentile depth of seismic events (D90 seismogenic depths) for cratonic earthquakes. Utilizing D90 instead of maximum depth extent can help mitigate the bias introduced by few deep earthquakes below the brittle zone that may not rupture at the surface, which can skew the depth measurements (Ruff and Kanamori, 1983). For our D90 measurements, we assigned 50% weighting to 13.5 km from the D90 depth histogram of earthquakes in the 2012 Australian Earthquake Hazard Map (Burbidge and Leonard, 2011); 25% weighting to 10.5 km 90th percentile depth from the Lake Eyre region earthquake catalog by Agrawal et al. (2024); 15% weighting to 5.82 km from the 90th percentile rupture depth extent of the Petermann earthquake (Attanayake et al., 2020); and 5% each to 21 km from the D90 seismogenic depth in the Flinders Ranges Seismic Zone (Balfour et al., 2015) and 3 km from the body wave analysis 90th percentile depth of surface rupturing Australian cratonic earthquakes (Jackson and McKenzie, 2022). The weighted average of these values resulted in an estimated D90 depth of 11.5 km, which we used to calculate down-dip rupture widths by dividing by the sine of dip angles for each fault. Subsequently, fault rupture area, the product of rupture width and rupture length, was calculated. Finally, we estimated the weighted maximum credible magnitudes (M_w max) for all length and area scaled magnitudes for our preferred, maximum, and segmented rupture scenarios.

4. Results

The current map (Figure 1) has been updated to include at least 10 definite splays and segments, and 13 probable and possible neotectonic features related to these faults, that have not been mapped in earlier studies (Miles, 1952; Parker, 1983a; Dunham, 1992; McCormack, 2006; Weatherman, 2006). This map incorporates locational uncertainty for geospatial mapping of the fault traces by adding confidence intervals (low – high) for the exact location of the fault, which often arises due to the resolution of the DEM dataset used and topographic noise.

This map provides a more detailed representation of fault traces compared to the Australian Neotectonic Features Database (Clark et al., 2012), which primarily relies on topographic relief or visibility from 30m DEMs. We have incorporated high resolution drone-derived DEMs to facilitate detailed mapping of specific field sites. The enhanced resolution helped identify previously undetected structures, splays, strands, and step-overs, providing a more comprehensive understanding of the area's neotectonic features (Figure 1; Figure 2). The accuracy of rupture tip locations was also improved by utilizing topographic offsets identified from our DEM datasets. By analysing perpendicular topographic profiles across the scarps, we were able to more precisely map the ends of the rupture traces. Moreover, the accuracy and confidence of our fault mapping was significantly improved by incorporating specific evidence of deformation of Quaternary sedimentary units in the north-eastern Eyre Peninsula.

4.1. Neotectonic Fault Scarps: Geospatial Analysis

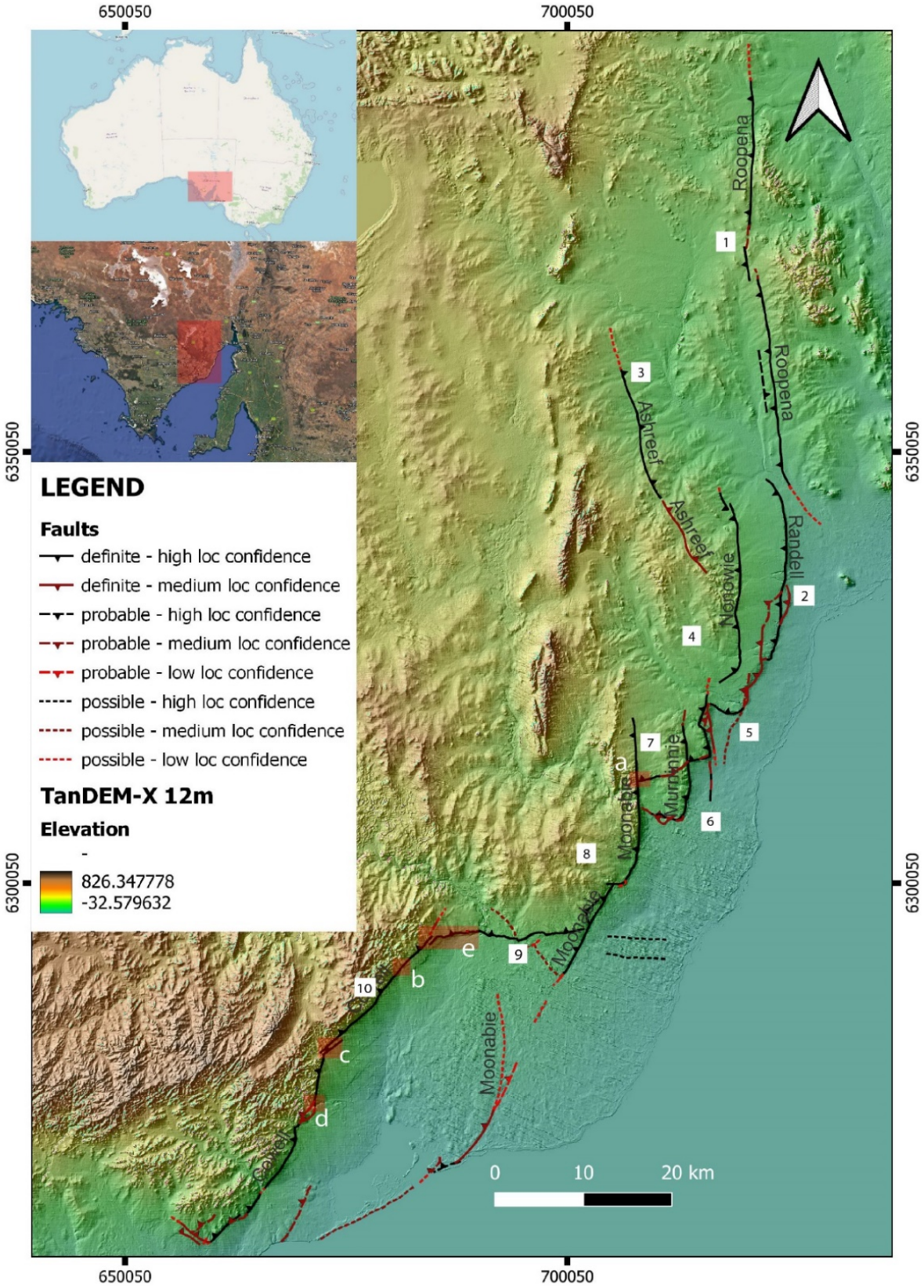

Figure 1: Updated map of the study area showing the definite, probable, and possible fault traces overlying the TanDEM-X 12 m dataset. Fault names: 1- Roopena, 2- Randell, 3- Ashreef, 4- Nonowie, 5-Poynton, 6- Murninnie N, 7- Murninnie Relay, 8- Moonabie, 9- Charleston, 10- Cowell. Sites a-e are shown in Figure 2 and show the locations of drone-derived DEMs.

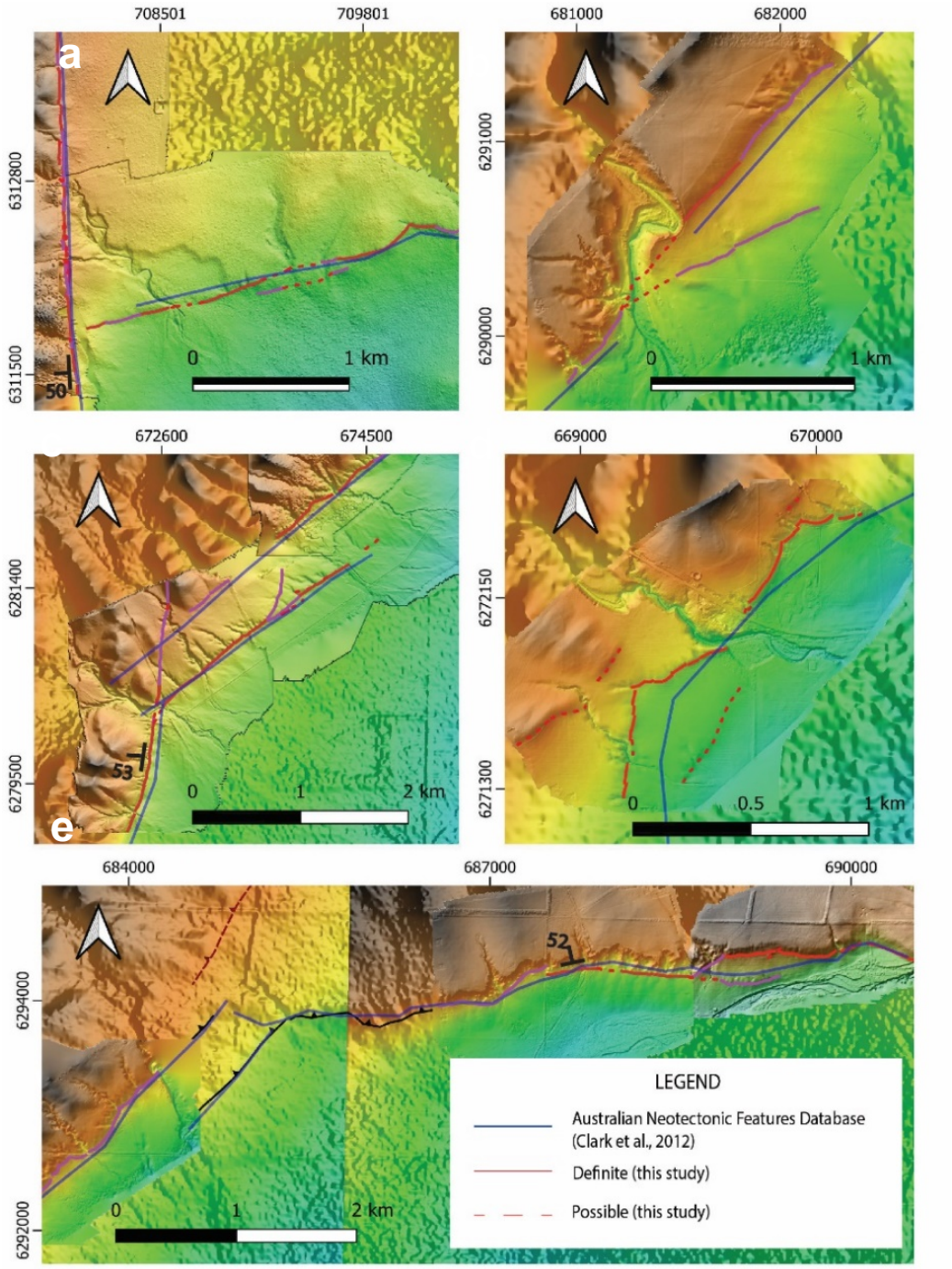

Figure 2: 7-15cm resolution drone derived DEMs collected during this study. The locations are shown in Figure 1. a) Intersection of N-S Moonabie fault with E-W Murninnie Relay; (b) Northernmost section of NE-SW Cowell fault with channel interactions; (c) Cowell fault and (interpreted) frontal thrust; (d) Cowell fault near Mindrow Creek; (e) E-W trending Charleston fault with NE-SW trending Cowell fault to the left. The bold blue traces depict the mapped traces in the current Australian Neotectonic Features Database (Clark et al., 2012).

4.2. Rupture Lengths and Role of Basement Structures

Maximum fault rupture length estimates range from 6 km to 73 km (Table 1) where we have conceptualised an ideal fault rupture encompassing all known and inferred fault segments that align with underlying geophysical lineaments along its strike. Surface lengths of individual segments range from 3 km to 27 km. Our preferred length estimates are based on detailed DEM and geophysical analysis of the geospatial dataset and a length uncertainty of ±5 km was incorporated to account for uncertainties pertaining to tips of the fault rupture and their discoverability in the DEMs. Our length estimates also include a simplified fault geometry for complex ruptures with splays and strands (e.g., Randell fault) or curved fault geometries (e.g., Poynton, and Murninnie faults).

Table 1: Summary of Surface Rupture Lengths from this study based on Preferred, Maximum, and Segmented Rupture Models. Lengths from previous studies (McCormack, 2006; Weatherman, 2006; Dunham,1992) have been shown.

Surface Rupture Lengths (km)										
Fault Name	Preferred Length ±5 km	Max Length	Segment lengths						SRL McCormack (2006); Weatherman (2006)	SRL Dunham (1992)
			A	B	C	D	E	F		
Roopena	48.3	73.8	23.4	24.8	7.0	8.6				26.4
Randell	32.9	42.9	32.9	7.0	3.8				37.4	27.4
Nonowie	22.8	25.0							20.7	19.2
Ash Reef	25.3	30.2								21.1
Poynton	22.1	23.8	22.1	4.5	4.4				11.8	25.1
Murninnie N	17.8	21.2							15.4	10.7
Murninnie Relay	6.1	6.1							5.9	
Moonabie	35.1	53.3	21.5	27.4	4.3	5.6				15.6
Charleston	18.2	18.2								
Cowell	46.2	57.0	18.5	21.3	2.7	7.6	3.4	3.1		

In order to investigate structural and spatial trends of the Eyre Peninsula faults and their relationship with the underlying basement structures, the rupture trace layer was superimposed on the total magnetic intensity map in QGIS (Figure 3). Our findings are as follows.

- The N-S trending continuous faults of the study area such as Roopena, Nonowie, Randell, Murninnie, and Moonabie, strike parallel to the underlying medium to high magnetic response geophysical lineaments. In some cases, these lineaments trend beyond the mapped fault traces.
- The E-W and N-S trending segments of the Poynton scarp follow the orientation of a broad-scale fold in the magnetic lineaments.
- While some segments of the E-W trending Charleston and Murninnie Relay faults appear to align with geophysical lineaments, others crosscut these structures, suggesting a complex fault system.
- The southernmost Cowell scarp strongly aligns with the high magnetic response lineaments of the underlying Kalinjala and Northcentral shear zones.

We estimate that out of 327 km of combined surface rupture lengths of these faults, up to 268.4 km (approximately 82%) aligns with underlying geophysical lineaments.

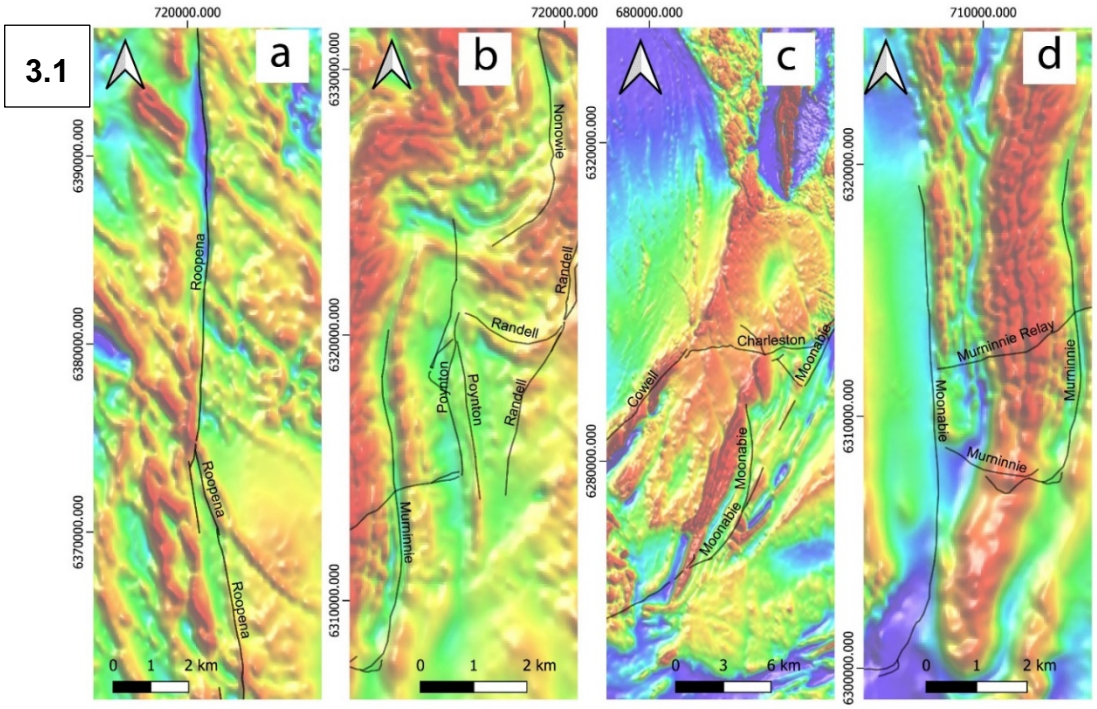

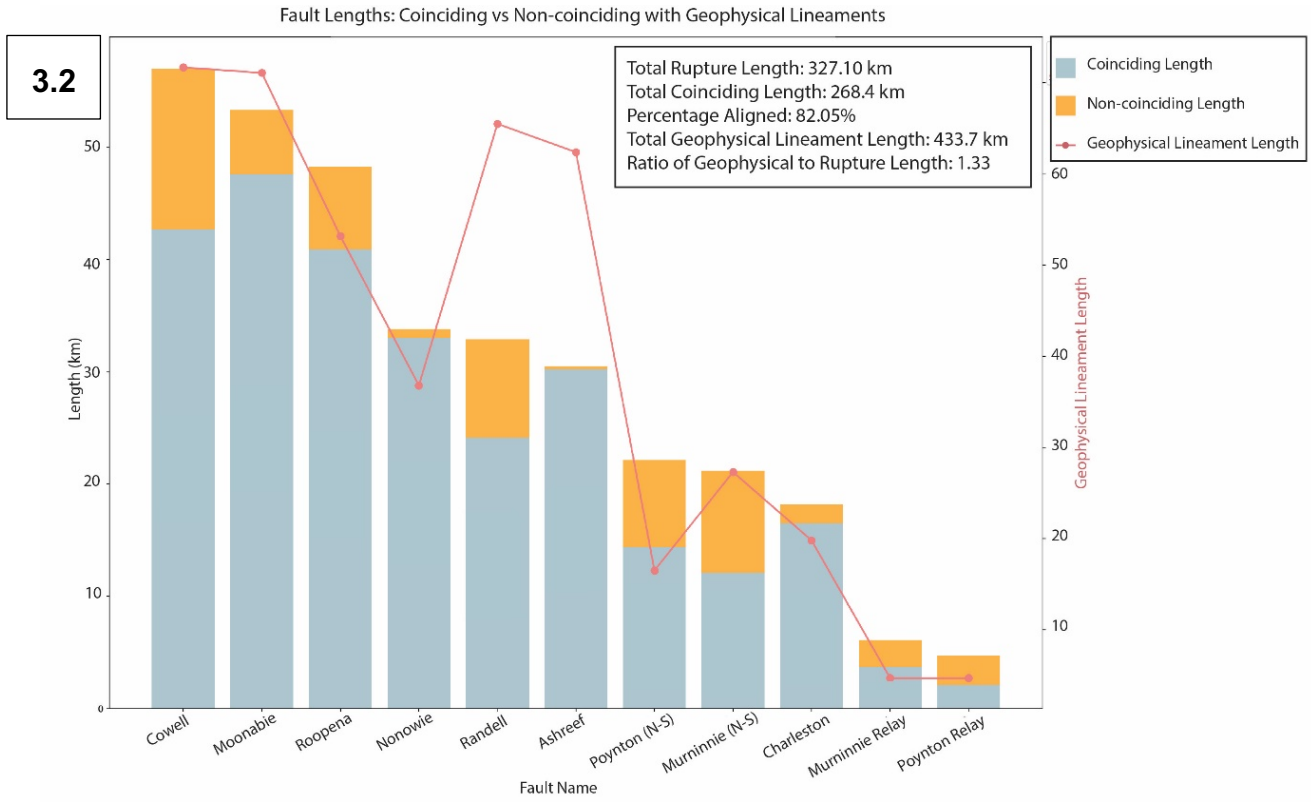

Figure 3.1: Maps a-d showing different fault rupture traces aligning with the orientations of geophysical lineaments in the total magnetic intensity dataset. Figure 3.2: Plot of coinciding vs non-coinciding rupture lengths of fault traces with the lengths of geophysical lineaments.

4.3. Fault Geometry, Seismogenic Depths, And Rupture Area

The down-dip rupture widths in our dataset were based on our weighted average D90 depth estimates of 11.5 km and near-surface dips of the Eyre Peninsula faults. For rupture area calculations, we selected the mode value of rupture widths. The rupture area estimates for our maximum rupture scenario range from 100 km^2 to 1108 km^2, while areas of individual segments range from 45 km^2 to 535 km^2. Our preferred rupture scenario area estimates range from 100 km^2 to 725 km^2 (Table 2). These area estimates were incorporated in area-based scaling relationships to estimate a M_w max for all faults and their individual segments.

Table 2: Summary of fault dips, down-dip rupture width (calculated from weighted average D90 seismogenic depth) and rupture area (product of rupture width and length) for preferred, maximum, and segmented rupture scenarios.

Fault Name	Fault Dip	+- Dip range	Down-Dip rupture width (km)	Uncertainty (km)*	Area (km sq)							
					Pref	Max	Segmented					
							A	B	C	D	E	F
Roopena	50	10	15.0	2.0	725.1	1107.9	350.8	372.3	105.1	129.1		
Randell	45	15	16.3	3.0	535.1	697.7	535.1	113.8	61.8			
Nonowie	45	15	16.3	3.0	370.8	406.1						
Ash Reef	45	15	16.3	3.0	411.1	491.3						
Poynton	45	15	16.3	3.0	360.2	386.3	360.2	73.2	71.2			
Murninnie N	50	10	15.0	2.0	267.8	318.3						
Murninnie Relay	45	15	16.3	3.0	100.0	100.0						
Moonabie	50	10	15.0	2.0	526.9	800.7	322.8	411.3	64.0	83.6		
Charleston	52	10	14.6	4.0	265.6	265.6						
Cowell	53	10	14.4	4.0	665.3	820.8	267.0	306.1	38.7	109.4	49.5	44.8

*The uncertainty values only represent uncertainties derived from fault dips and do not include uncertainties associated with down-dip rupture width estimates, for the purpose of this analysis.

4.4. Scaling Relationships and Maximum Credible Earthquake Moment Magnitudes

4.4.1. Length-Scaled Magnitudes

Length scaled magnitudes were derived using the Yang et al. (2021) and Leonard (2014) scaling relationships between surface rupture length (SRL) and M_w.

Our M_w estimates using the regressions from Yang et al. (2021) (Table 3) for the preferred rupture scenario M_w range from 5.4 to 7.2, and 5.4 to 7.6 for the tip-to-tip rupture scenario. The segmented length-based M_w range from 4.7 to 6.9.

Likewise, M_w estimates using Leonard (2014) regressions (Table 3) range from 5.6 to 7.1 for the preferred rupture scenario and 5.6 to 7.4 for the tip-to-tip ruptures, while the M_w for each segment length ranged from 5.1 to 6.8.

Table 3: Summary of length scaled maximum credible moment magnitudes (Mw) for preferred, maximum, and segmented rupture scenarios from Yang et al., (2021) and Leonard (2014) scaling relationships.

Fault Name	Length-scaled Max Moment Magnitude (Yang et al., 2021)								Length-scaled Max Moment Magnitude (Leonard 2014)							
	Pref	Max	Segmented						Pref	Max	Segmented					
			A	B	C	D	E	F			A	B	C	D	E	F
Roopena	7.2	7.6	6.6	6.6	5.6	5.7			7.1	7.4	6.6	6.6	5.7	5.9		
Randell	6.9	7.1	6.9	5.6	5.0				6.8	7.0	6.8	5.7	5.3			
Nonowie	6.6	6.7							6.6	6.6						
Ash Reef	6.7	6.8							6.7	6.8						
Poynton	6.6	6.6	6.6	5.2	5.1				6.6	6.6	6.6	5.4	5.4			
Murninnie N	6.4	6.5							6.4	6.5						
Murninnie Relay	5.4	5.4							5.6	5.6						
Moonabie	7.0	7.3	6.5	6.7	5.1	5.4			6.9	7.2	6.5	6.7	5.4	5.6		
Charleston	6.4	6.4							6.4	6.4						
Cowell	7.2	7.4	6.4	6.5	4.7	5.6	4.9	4.8	7.1	7.2	6.4	6.5	5.0	5.8	5.2	5.1

4.4.2. Area-Scaled Magnitudes

M_w derived from area-based regressions from Leonard (2014) and Somerville (2014) utilised the area (km sq) calculated for each rupture scenario (Preferred, Max and Segmented) (Table 2).

Our M_w estimates using the regressions from Leonard (2014) (Table 3) for the preferred rupture scenario M_w range from 6.2 to 7.1, and 6.2 to 7.2 for the tip-to-tip rupture scenario, while the segmented scenario M_w range from 5.8 to 6.8.

M_w estimates from Somerville (2014) (Table 4) range from 6.3 to 7.1 for the preferred rupture scenario and 6.3 to 7.3 for the tip-to-tip ruptures. Our Somerville (2014) M_w range for the segmented scenario is from 5.9 to 7.0.

Table 4: Summary of area scaled maximum credible moment magnitudes (Mw) for preferred, maximum, and segmented rupture scenarios from Leonard (2014) and Somerville (2014) scaling relationships.

Fault Name	Area-scaled Max Moment Magnitude (Leonard 2014)								Area-scaled Max Moment Magnitude (Somerville 2014)							
	Pref	Max	Segmented						Pref	Max	Segmented					
			A	B	C	D	E	F			A	B	C	D	E	F
Roopena	7.1	7.2	6.7	6.8	6.2	6.3			7.1	7.3	6.8	6.8	6.3	6.4		
Randell	6.9	7.0	6.9	6.2	6.0				7.0	7.1	7.0	6.3	6.0			
Nonowie	6.8	6.8							6.8	6.9						
Ash Reef	6.8	6.9							6.9	6.9						
Poynton	6.7	6.8	6.7	6.1	6.0				6.8	6.8	6.8	6.1	6.1			
Murninnie N	6.6	6.7							6.7	6.8						
Murninnie Relay	6.2	6.2							6.3	6.3						
Moonabie	6.9	7.1	6.7	6.8	6.0	6.1			7.0	7.2	6.8	6.9	6.1	6.2		
Charleston	6.6	6.6							6.7	6.7						
Cowell	7.0	7.1	6.6	6.7	5.8	6.2	5.9	5.8	7.1	7.2	6.7	6.7	5.8	6.3	5.9	5.9

4.4.3. Weighted Magnitudes from Scaling relationships

Table 5: Summary of weighted scaled maximum credible moment magnitudes (Mw) for preferred, maximum, and segmented rupture scenarios from length and area-based scaling relationships. Weighting for L<=40 km: Yang L Mw 0.4, Leonard L Mw 0.4; Leonard A Mw 0.1; Somerville A Mw 0.1. Weighing for L>40 km: Yang L Mw 0.05, Leonard L Mw 0.15; Leonard A Mw 0.4, Somerville A Mw 0.4.

Fault Name	Pref	Max	Uncertainty (+/-)	Weighted Max Mw (Length and Area) Segmented					
				A	B	C	D	E	F
Roopena	7.1	7.3	0.2	6.7	6.8	6.1	6.2		
Randell	6.9	7.1	0.2	6.9	5.8	5.3			
Nonowie	6.6	6.7	0.2						
Ash Reef	6.7	6.8	0.2						
Poynton	6.6	6.7	0.2	6.6	5.4	5.4			
Murninnie N	6.4	6.6	0.2						
Murninnie Relay	5.7	5.7	0.2						
Moonabie	6.9	7.2	0.2	6.6	6.7	5.4	5.6		
Charleston	6.4	6.4	0.2						
Cowell	7.1	7.2	0.2	6.6	6.7	5.6	6.2	5.8	5.7

Based on our weighted maximum credible moment magnitude (M_w) calculations from length and area scaling relationships, the segmented M_w potentials range from 5.3 to 6.9 and tip-to-tip rupture M_w potentials range from 5.7 to 7.3.

The weighted scaled M_w calculations also incorporate epistemic uncertainties in the scaling relationships used. Regressions based on historical Australian earthquakes are deemed more reliable in the context of Eyre Peninsula faults due to the region's similar cratonic crust and crystalline basement. We favour Yang et al. (2021) regressions for rupture lengths less than 40 km, owing to the fact that Yang et al. (2021) scaling relationships for length-based Mw calculations for SCR earthquakes are limited to surface rupture lengths for historical Australian earthquakes not exceeding lengths of 40 km (e.g., 1968, Meckering). Therefore, magnitude estimates for lengths above 40 km would have to be interpolated for this regression. In order to avoid interpolating and increasing the uncertainty associated with it, we allocate a higher weighting (75%) to Leonard (2014) length scaled magnitudes for faults with lengths >40 km. Length scaled magnitudes for faults with lengths <40 km have been weighted equally for both Yang et al. (2021) and Leonard (2014) regressions. It is important to emphasize that due to the higher degrees of epistemic uncertainties in our estimation of weighted average seismogenic depths, we weigh the length-based regressions slightly higher than the area-based regressions in our weightings. To account for the diverse nature of uncertainty in our weighted M_w dataset, we apply a +/- 0.2 M_w uncertainty to all M_w max estimations. Future work will aim at better defining the uncertainties using Monte Carlo simulations to sample across a range of plausible rupture depths.

5. Discussion

High resolution DEM based detailed mapping helped with providing precise locations and geometries of faults, along with the addition of smaller structures that were not previously visible in the 30m DEM datasets. Most of the Eyre Peninsula fault traces exhibit a linear strike, nearly normal to the contemporary NW-SE oriented SHmax of the region (Rajabi et al., 2017). These north trending faults follow an arcuate shape towards their southern tip where the trace

curves to an east-west trending structure that parallels the geophysical lineaments observed in the magnetic intensity dataset. This arcuate shape is highly similar to other historic surface ruptures, e.g., 1986 Marryat Creek – an arcuate rupture with two intersecting geophysical lineaments, and the 1968 Meckering rupture (Vogfjörd & Langston, 1987; Machette et al., 1993). While the E-W trending fault traces such as the Murninnie Relay and the Charleston ruptures are not strictly coincident with the strongly magnetic lineaments, they are constrained by displaced N-S trending magnetic highs (Figure 3**Error! Reference source not found.**A). The strongly arcuate limb of the Randell fault also parallels a N-S to E-W trending broad-scaled fold within the magnetic dataset.

Although there are no constraints on the depth or dips of these magnetic lineaments, field measurements from outcrops of mylonitic bedrocks along the Cowell and Moonabie faults are in approximate congruence with the measurements of strikes and dips of these neotectonic fault traces. Our analysis of rupture lengths indicates that approximately 82% of the total rupture lengths align with the lengths of underlying geophysical lineaments. These geophysical structures may be associated with basement fractures, dikes, or underlying basement faults, indicating the role of pre-existing crustal architecture that influences the location and geometry of the Eyre Peninsula surface ruptures. Hence, some of our estimations for fault dips, particularly in areas with limited exposure, are based on the known dips of these structures assuming that these bedrock fabrics may represent reactivated zones of crustal weakness formed during the Paleoproterozoic Kimban orogeny that were favourably aligned to rupture within the neotectonic NW-SE compressive stress regime.

Our measurements of rupture lengths for our preferred rupture scenarios also assume a simplified rupture trace (e.g., Poynton and Poynton Relay faults). While the Poynton and Poynton Relay faults have been mapped as separate structures in previous studies (Miles, 1952; Dunham, 1992; McCormack 2006; Weatherman, 2006), we favour a conservative M_w max based rupture scenario where these curved faults (Randell, Poynton, Poynton Relay, Murninnie) represent highly curved and continuous geometries, similar to the Marryat Creek earthquake (Crone et al., 1997). Topographical vertical offsets from the Poynton and Poynton Relay scarp range from 30-40m, with geomorphic ages as suggested by McCormack (2006) indicating the possibility of multiple rupture events. To incorporate this epistemic uncertainty, our segmented rupture scenarios based on strike variations of more than 25^0, and proximity to other traces (≤ 2 km) divide the curved Poynton and Poynton Relay trace into 3 different segments, with lengths ranging from 4.4 to 22 km. Similarly, a N-S trending simplified rupture length is assumed for the Randell scarp where the multiple N-S oriented splays strongly align with magnetic highs in the geophysical dataset (Figure 3A). Preliminary Bouguer gravity analysis by Weatherman (2006) indicates the presence of a competent Hiltaba Suite granitoid that may have acted as a rupture barrier causing strain partitioning into multiple splays. The exact rupture lengths are likely to be longer than the simplified lengths of the surface rupture as the fault may not have ruptured along its complete length to the surface. This may explain the variation of lengths compared to the Australian Neotectonic Features Database (Clark and McPherson, 2012).

Weighted M_w estimates for the Eyre Peninsula faults have been calculated based on the preferred weighting assigned to scaling relationships derived from historical Australian surface ruptures (Yang et al., 2021) and dip-slip faults from analogous stable continental regions (Leonard, 2014; Somerville, 2014). These weighted maximum credible magnitude estimates range from 5.7 to 7.3 for our preferred and maximum segmentation scenarios. Taking into account the magnitude estimates from Australian SCR faults (Clark et al., 2012; Quigley et al., 2006), we consider these estimates from the Eyre Peninsula region to be reasonable, given the longer recurrence intervals of these events (10k to 100k years) (Crone et al., 1997) and the short historical seismic records from Australia. Considering the potential for erosion or removal of scarp tips and the influence of fluvial geomorphology on fault trace visibility, our estimated magnitude values should be interpreted as minimum bounds for earthquake magnitudes in the Eyre Peninsula. Although, if the true D90 depth for Eyre Peninsula faults is shallower than our weighted average, these magnitudes would be an over-estimation.

Subsequent work will consider a range of plausible rupture depths using Monte Carlo simulations to address this uncertainty more effectively.

6. Future work

Future studies will focus on quantifying single-event displacements and analysing fault segmentation scenarios through shape fitting of displacement distribution profiles. Additionally, we aim to determine the ages of the last faulting events on individual Eyre Peninsula faults through Optically Stimulated Luminescence (OSL) age estimates from paleoseismic trenching, and other samples collected across the region and assess the long term and localised slip rates. These efforts will further enhance the PSHA and PFDHA models by refining the fault source models for the Eyre Peninsula by incorporating additional data and reducing both aleatoric and epistemic uncertainties associated with the region's faults

7. Acknowledgements

This research was funded by the Australian Government National Emergency Agency (NEMA) Disaster Ready Fund (Project DRF 40204) and by AuScope (Project 3.128) via the National Collaborative Research Infrastructure Strategy (NCRIS). The authors would also like to thank the Barngarla Traditional Owners of the land and all the private landowners for their time and for allowing us access to their properties in Eyre Peninsula.

8. References

Agrawal, S., Eakin, C. M., & O'Donnell, J. P. (2024). Fluid-assisted intra-plate seismicity at the edge of the Gawler Craton, South Australia. *Physics of the Earth and Planetary Interiors*, *346*, 107133.

Allen, T. I. (2020). Seismic hazard estimation in stable continental regions: Does PSHA meet the needs for modern engineering design in Australia? *Bulletin of the New Zealand Society for Earthquake Engineering*, *53*(1), pp. 22-36.

Allen, T. I., Griffin, J. D., Clark, D. J., Cummins, P. R., Ghasemi, H., & Ebrahimi, R. (2023). The 2023 National Seismic Hazard Assessment for Australia.

Allen, T. I., Griffin, J. D., Leonard, M., Clark, D. J., & Ghasemi, H. (2020). The 2018 national seismic hazard assessment of Australia: Quantifying hazard changes and model uncertainties. *Earthquake Spectra*, *36*(1_suppl), 5-43.

Alley N.F. & Lindsay J.M. (1993). Pirie Basin. In: Drexel J.F., and Preiss W.V. eds. The Geology of South Australia, Volume 2: The Phanerozoic, Mines and Energy, South Australia, Geological Survey of South Australia Bulletin 54, pp. 175-178.

Alexander, E. (2023). Natural Hydrogen in South Australia.

Attanayake, J., King, T. R., Quigley, M. C., Gibson, G., Clark, D., Jones, A., ... & Sandiford, M. (2020). Rupture characteristics and bedrock structural control of the 2016 M w 6.0 intraplate earthquake in the Petermann Ranges, Australia. *Bulletin of the Seismological Society of America*, *110*(3), pp. 1037-1045.

Balfour, N. J., Cummins, P. R., Pilia, S., & Love, D. (2015). Localization of intraplate deformation through fluid-assisted faulting in the lower-crust: The Flinders Ranges, South Australia. *Tectonophysics*, *655*, 97-106.

Biasi, G. P., & Wesnousky, S. G. (2017). Bends and ends of surface ruptures. *Bulletin of the Seismological Society of America*, *107*(6), pp. 2543-2560.

BHP Minerals Ltd. (1983). EL 766 Mullaquana, Progress and Final Reports for the Period 8/12/80 to 7/12/82, Open File Envelope No. 4124. Primary Industries and Resources South Australia (PIRSA) 1983.

Burbidge, D., & Leonard, M. (2011). The 2012 Australian seismic hazard map–Draft maps. In *Australian Earthquake Engineering Society 2011 Conference* (pp. 18-20).

Célérier, J., Sandiford, M., Hansen, D.L., Quigley, M. (2005). Modes of active intraplate deformation, Flinders Ranges, Australia, Tectonics 24 (6).

Chartier, T., Scotti, O., Clément, C., Jomard, H., & Baize, S. (2017). Transposing an active fault database into a fault-based seismic hazard assessment for nuclear facilities–Part 2: Impact of fault parameter uncertainties on a site-specific PSHA exercise in the Upper Rhine Graben, eastern France. *Natural Hazards and Earth System Sciences*, *17*(9), pp. 1585-1593.

Clark, D., McPherson, A. (2012). Neotectonic Features Database. https://pid.geoscience.gov.au/dataset/ga/74056

Clark, D., McPherson, A., & Van Dissen, R. (2012). Long-term behaviour of Australian stable continental region (SCR) faults. *Tectonophysics*, *566*, pp. 1-30.

Clark, D., McPherson, A., Allen, T., & De Kool, M. (2014). Coseismic surface deformation caused by the 23 March 2012 M w 5.4 Ernabella (Pukatja) earthquake, central Australia: Implications for fault scaling relations in cratonic settings. *Bulletin of the Seismological Society of America*, *104*(1), 24-39.

Clark D., Van Dissen R., Cupper M., Collins C. & Prendergast A. (2007). Temporal clustering of surface ruptures on stable continental region faults: a case study from the Cadell Fault scarp, southeastern Australia. Paper presented at Australian Earthquake Engineering Society Conference, Wollongong (unpubl.).

Clark, D., Leonard, M., Griffin, J., Stirling, M., & Volti, T. (2016, November). Incorporating fault sources into the Australian National Seismic Hazard Assessment (NSHA) 2018. In *Australian Earthquake Engineering Society 2016 Conference*.

Cornell, C. A. (1968). Engineering seismic risk analysis. *Bulletin of the seismological society of America*, *58*(5), pp. 1583-1606.

Crone, A. J., Machette, M. N., & Bowman, J. R. (1993). Geologic Investigations of the 1988 Tennant Creek, Australia, Earthquakes--Implications for Paleoseismicity in Stable Continental Regions: Investigations of the Paleoseismology, Deformation, and Quaternary Stratigraphy Associated with Reverse Faulting Caused by Three Major Earthquakes in the Interior of the Australian Craton (No. 2032). US Government Printing Office.

Crone A. J. & Machette M. N. (1997). The temporal variability of surface-faulting earthquakes in stable continental regions; a challenge to seismic-hazard assessments. Abstracts with Programs - Geological Society of America 29, 71.

Crone A. J., De Martini P. M., Machette M. N., Okumura K. & Prescott J. R. (2003). Paleoseismicity of Two Historically Quiescent Faults in Australia: Implications for Fault Behavior in Stable Continental Regions. Bulletin of the Seismological Society of America 93, pp. 1913-1934.

Department of State Development, South Australia. (n.d.). Hydrogen projects in South Australia. (Retrieved from https://www.hydrogen.sa.gov.au/industry/hydrogen-projects-in-south-australia)

Dunham M. N. E. (1992). The geomorphological nature and age of the linear escarpments of north-eastern Eyre Peninsula, University of Adelaide, (unpublished).

Hanžl, Pavel & Verner, Krystof & Buriánek, David & Šíma, Jiří & Janderkova, Jana & Paleček, Martin & Hroch, Tomáš & Martínek, Karel & Megerssa, Leta & Hrdličková, Kristýna & Metelka, Vaclav. (2019). Basic principles of geological and thematic mapping, pp 47-48.

Jackson, J., & McKenzie, D. (2022). The exfoliation of cratonic Australia in earthquakes. Earth and Planetary Science Letters, *578*, 117305.

Jessup R. W. & Wright M. J. (1971). Cenozoic sediments, soils and climates at Whyalla, South Australia. Geoderma 6, pp. 275-308.

King, T., Quigley, M., & Clark, D. (2019a) The 30th March 1986 Mw 5.7 Marryat Creek surface rupturing earthquake, Australia.

King, T., Quigley, M., & Clark, D. (2019b). The 14th October 1968 Mw 6.6 Meckering surface rupturing earthquake, Australia.

King, T., Quigley, M., & Clark, D. (2019c). The 20th May 2016 Mw 6.1 Petermann surface rupturing earthquake, Australia.

King, T. R., Quigley, M., & Clark, D. (2019d). Surface-rupturing historical earthquakes in Australia and their environmental effects: New insights from re-analyses of observational data. *Geosciences*, *9*(10), 408.

Leonard, M. (2014). Self-consistent earthquake fault-scaling relations: Update and extension to stable continental strike-slip faults. *Bulletin of the Seismological Society of America*, *104*(6), 2953-2965.

Ludbrook, N.H. (1959). A widespread Pliocene molluscan fauna with Anodontia in South Australia. Royal Society of south Australia. Transactions, 82, pp. 219-234.

Machette, M. N., Crone, A. J., & Bowman, J. R. (1993). Geologic investigations of the 1986 Marryat Creek, Australia, earthquake: implications for paleoseismicity in stable continental regions (No. 2032). US Government Printing Office.

Matsuda, T. (1990). Seismic zoning map of Japanese islands, with maximum magnitudes derived from active fault data. Bulletin of Earthquake Reseach Institute, 65, pp. 289-319.

McCormack B.J. (2006). Quaternary Fault Scarps on the North-eastern Eyre Peninsula, South Australia; Geomorphic constraints on age and faulting history by investigation of knickpoint retreat. The University of Melbourne, Honours thesis (unpublished).

Miles, K.R. (1954). The geology and iron ore resources of the Middleback Range area. South Australia. Geological Survey. Bulletin, 33.

Miles, K. R., 1952. Tertiary faulting in north-eastern Eyre Peninsula, South Australia, Transactions of the Royal Society of South Australia, 75, 89-96.

Parker, A. J., Webb, A. W., Fanning, C. M., Oliver, R. L., Cooper, J. A., Daly, S., ... & Goode, A. D. T. (1980). Symposium on the Gawler Craton, 11 December 1979.

Parker, A.J. (1983a). WHYALLA map sheet. South Australia. Geological Survey. Geological Atlas 1:250 000 Series, sheet SI53-8.

Parker A.J., and Lemon N.M. (1982). Reconstruction of the early Proterozoic stratigraphy of the Gawler Craton, South Australia. Journal of the Geological Society of Australia 29, pp. 221-238.

Parker, A. J., Fanning, C. M., & Flint, R. B. (1985). Geology. In C. R. Twidale, M. J. Tyler, & M. Davies (Eds.), Natural history of Eyre Peninsula, Royal Society of South Australia, pp. 21-45.

Parker A.J., and Fanning C.M. (1998). Explanatory Notes for the WHYALLA 1:250 000 Geological Map, Primary Industries and Resources South Australia.

Quigley, M.C., Cupper, M.L., Sandiford, M. (2006) Quaternary faults of south-central Australia: Palaeoseismicity, slip rates and origin, Australian Journal of Earth Sciences, 53, pp. 285–301.

Rajabi, M., Tingay, M., Heidbach, O., Hillis, R., Reynolds, S. (2017) The present-day stress field of Australia, Earth-Science Reviews, 168, pp. 165–189.

Ruff, L., and H. Kanamori (1983). Seismic coupling and uncoupling at subduction zones, Tectonophysics, 99(2), pp. 99–117.

Sellmann, S., Quigley, M., Duffy, B., Yang, H., & Clark, D. (2023). Fault geometry and slip rates from the Nullarbor and Roe Plains of south-central Australia: Insights into the spatial and temporal characteristics of intraplate seismicity. *Earth Surface Processes and Landforms*, *48*(2), pp. 350-370.

Somerville (2014). Scaling relations between seismic moment and rupture area of earthquakes in stable continental regions. Report to the NGA-East Project, PEER 2014/14, August. Berkeley, CA: Pacific Earthquake Engineering Research Center.

Somerville, P. (2021). Scaling relations between seismic moment and rupture area of earthquakes in stable continental regions. Earthquake Spectra, 37(1_suppl), pp. 1534-1549. https://doi.org/10.1177/8755293020988024

Thom, B., Hesp, P., & Bryant, E. (1994). Last glacial “coastal” dunes in Eastern Australia and implications for landscape stability during the Last Glacial Maximum. *Palaeogeography, Palaeoclimatology, Palaeoecology*, *111*(3-4), pp. 229-248.

Vassallo, J. J., & Wilson, C. J. L. (2001). Structural repetition of the Hutchison Group metasediments, Eyre Peninsula, South Australia. *Australian Journal of Earth Sciences*, *48*(2), pp. 331-345.

Vassallo, J.J. and Wilson, C.J.L., (2002). Palaeoproterozoic regional-scale non-coaxial deformation: an example from eastern Eyre Peninsula, South Australia. Journal of Structural Geology, 24(1), pp. 1-24.

Vassallo J.J., and Wilson C.J.L. (1999). The Great Southern Transect II. Part 2. Palaeoproterozoic geology of southeastern Eyre Peninsula. In: Wilson C.J.L. ed. The Great Southern Transect 2, Geological Society of Australia, Specialist Group in Tectonics and Structural Geology, Field Guide 6, pp. 34-79.

Vogfjörd, K. S., & Langston, C. A. (1987). The Meckering earthquake of 14 October 1968: A possible downward propagating rupture. *Bulletin of the Seismological Society of America*, *77*(5), 1558-1578.

Weatherman, M. L. B. (2006). Basement Control on Distribution of Active Faults on Northeastern Eyre Peninsula, and some Seismic Implications, University of Melbourne, (unpublished).

Webb, A. W. (1980). A geochronological investigation of the tectono-magmatic history of the Gawler Craton. *Journal of the Geological Society of Australia*, 27, pp. 45-46.

Wells, D., & Coppersmith, K. (1994). New Empirical Relationships among Magnitude, Rupture Length, Rupture Width, Rupture Area, and Surface Displacement. Bulletin of the Seismological Society of America, 84(4), pp. 974-1002.

Yang, H., Quigley, M. and King, T. (2021). Surface slip distributions and geometric complexity of intraplate reverse-faulting earthquakes. GSA Bulletin, 133(9-10), pp.1909- 1929.